Arch. Metall. Mater. **66** (2021), 3, 917-924

DOI: 10.24425/amm.2021.136398

MUSA KİLİÇ[1*]

MICROSTRUCTURAL CHARACTERIZATION OF Ni-BASED B_4C REINFORCED COMPOSITE COATING PRODUCED BY TUNGSTEN INERT GAS METHOD

In this study, NiCrBSi-B_4C (wt. %5, %10 ve %15 B_4C) powder mixtures are coated on the stainless steel surface of AISI304 by tungsten inert gas (TIG) method. We use optic microscope and scanning electron microscope (SEM) for the coating layer analysis, energy dispersive spectrometry (EDS) for element distribution analysis and X-ray diffractogram (XRD) for the analysis of phase components. The measurements of hardness are determined by the microhardness tester. Based on the results obtained by the examination of microstructure and phases, it has been observed that while B and C elemets are more intense in the middle and upper parts of the coating layer, the parts close to the interface have a higher intensity of Ni and Fe. Moreover, there are phases such as Cr_7C_3, γ – Ni, CrFeB, Ni_3B, CrB ve Fe_2B are formed in the coating layer. The increasing ratio of B_4C results in increasing on the measurement values of microhardness. The maximum hardness value (430,8 $HV_{0.2}$) is obtained from the coating layer of S4 sample while the minimum value (366,9 $HV_{0.2}$) is observed from the NiCrBSi coated sample.

Keywords: Coating, NiCrBSi-B_4C, Cr_7C_3, Microstructure, Microhardness

1. Introduction

In many engineering applications, corrosion, wear, fracture, and fatigue are encountered as problems that significantly affect the surface properties of materials. Production of wear-resistant materials by strengthening the surface properties of metallic materials with composite coatings has become a very important situation. Metal matrix composite (MMC) coatings have been developed to benefit from both the hardness of carbides and the toughness of metals. In recent years, studies have been conducted to improve the surface properties of materials with many production methods such as coating with high-velocity oxy-fuel (HVOF) spray coating, plasma spraying, laser coating, plasma coating, and tungsten inert gas (TIG) method in production of MMC coating. Due to the presence of a metallurgical bonding between the coating and the substrate, high porosity ratio in the coating layer and thickness of coating layer limited up to a few hundred micrometers in plasma spray and HVOF coatings, its usage is limited [1]. Although obtaining a microstructure with finer grains due to high heating and cooling rates in laser coating method as well as a heat affected zone in a much smaller area by less damage of the high power density to the substrate are an advantage, requiring very special conditions and very high equipment and protection cost in powder coatings have limited its applicability [2,3]. Coatings made with tungsten inert gas (TIG), laser, plasma arc welding (PTA) methods for the production of MMK composite coatings provide deeper penetration comparing to the other coating methods. Moreover, TIG coating process is a low cost and much easier to use in the atmosferic environment and also easier to control the thickness, chemical composition and properties of the coating compared to other processes [4]. TIG coating/alloying is an alternative way to coat ceramics having very high melting temperature on surface of metallic substrates with the surface layer developed by melting powder or powder mixtures previously placed on the substrate surface [5]. Melting the metallic powders previously placed on the surface of metal to be coated is due to the arc forming between the material and the tungsten electrode in the TIG welding torch and it allows a metallurgical bond between the melting and rapidly solidifying coating layer and the substrate [6]. A high-quality hard coating layer with improved mechanical properties can be produced by forming fine grained microstructures through rapid solidification.

Nickel-based alloys, especially NiCrBSi alloys, are widely used in various industrial areas in terms of the coating materials produced with thermal spraying and melting methods due to their low density, relatively high resistance against fracture [7],

[1] BATMAN UNIVERSITY, FACULTY OF TECHNOLOGY, DEPARTMENT OF MANUFACTURING ENGINEERING, BATMAN, TURKEY

Corresponding author: musa.kilic@batman.edu.tr

high bond strength, and excellent corrosion and wear resistance [8]. B in the chemical composition of NiBSi and NiCrBSi based alloy powders lowers the melting point and increases the hardness of the alloy by forming hard phase such as Ni_3B by combining with Ni [9]. Si is added to improve the fluidity of the nickel. In previous studies, it was stated that addition of Si into Ni in a constant amount of B reduced the liquid temperature of the alloy [10]. Cr provides high resistance against oxidation and high temperature corrosion [11,12]. In addition, it also improves the wear resistance and mechanical properties by means of the compounds and phases it forms with other elements in order to produce hard precipitates [13].

In this study, NiCrBSi and B_4C powder mixtures previously placed on surface of AISI304 stainless steel were melted with TIG coating process and NiCrBSi-B_4C MMC coating layer was produced. Microstructure and element analysis of MMC coating layer were evaluated with SEM and EDS analysis. Phase components of coating layers were determined with X-ray diffraction (XRD) method. The hardness was measured using a microhardness device and correlated with the microstructure obtained on the coated surface.

2. Experimental Study

In this study, surface of AISI 304 stainless steel was coated with TIG method. The purpose of the study is to determine and characterize the phases with microstructures forming on the surface layer of the previously coated steel material.

In order to coat NiCrBSi-B_4C composite material with TIG method, 80×20×10 mm^3 AISI 304 stainless steel plates were used as the substrate material. The surface of the steel plates was polished with 220 grit SiC sandpaper and cleaned with ethyl alcohol to avoid any dirt and residue. In order to place the coating powders, channels with 8 mm width and 1.5 mm depth were opened on the substrates. The powders used in the coating were B_4C (average grain size ~45 µm) and NiCrBSi (grain size ~50-150 µm) powders. The chemical composition (mass, %) of NiCrBSi powder was 18.76% Cr, 6.72% B, 3.01% Si and the rest was Ni. Chemical composition of B_4C powder was 57.23% B and 42.77% C. Figure 1 shows SEM morphology and EDS data of the powders used in the study. As seen in Figure 1 (a), while NiCrBSi powders were spherical, B_4C powders had a sharp and pointed corner mosaic appearance (Fig. 1(b)).

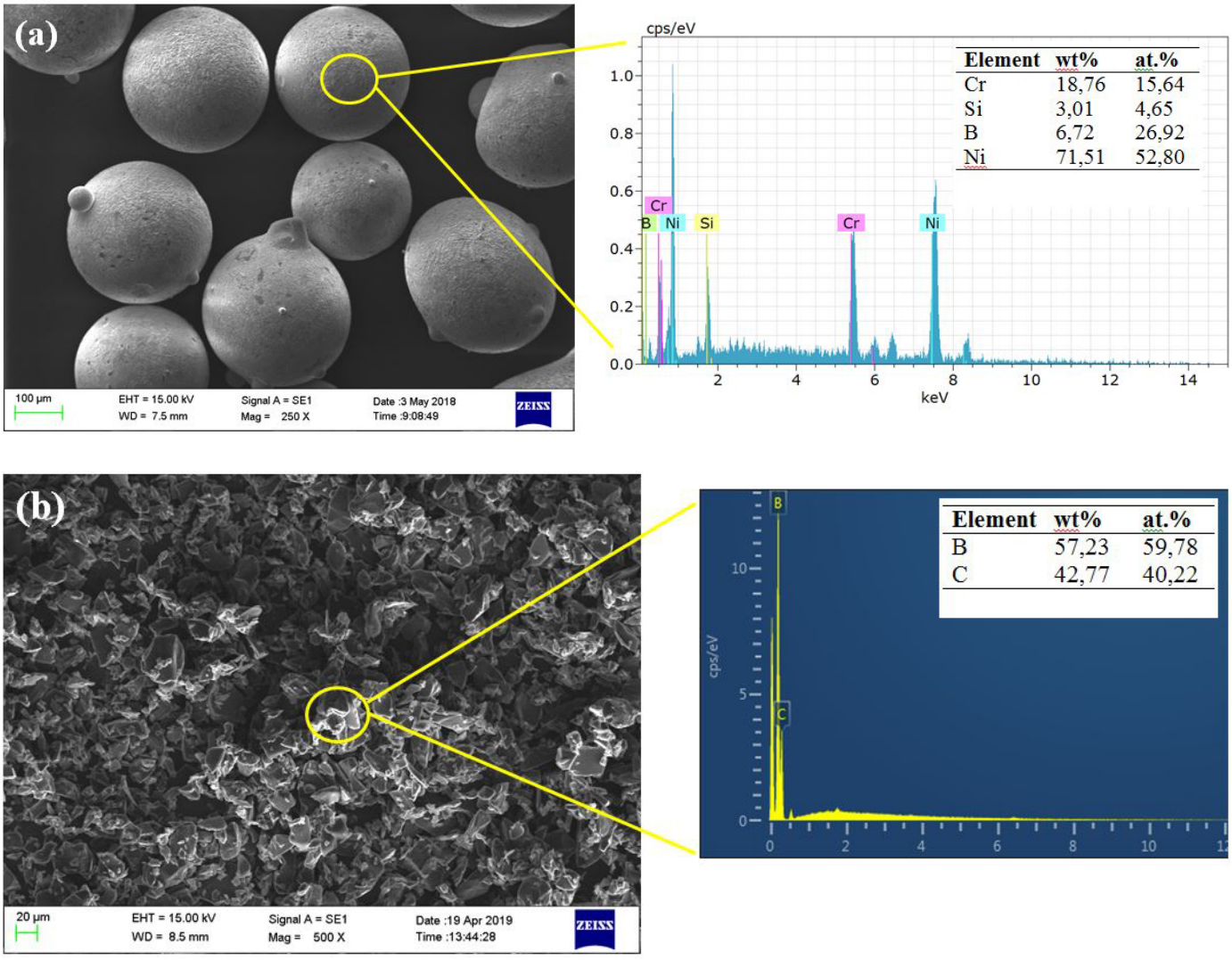

Fig. 1. Morphologies of the powders used in coating; (a) NiCrBSi powder and (b) B_4C powder

B_4C particles were added into NiCrBSi powders in the weight rates of 5%, 10%, and 15%. The mixture was prepared by mixing with 10:1 ceramic balls at 60 rpm for 2 hours with a special powder mixing apparatus. The powders were distributed homogeneously on the stainless steel layer by forming a semi-solid solution with polyvinyl alcohol and dried at room temperature for 24 hours in order to evaporate the binder and thus obtain a dry powder mixture.

For surface coating, tungsten inert gas (TIG) (Oerlikon-Magic Wave 2200) welding machine was used as the heat sources. The gap between the previously placed powder layer and the tungsten electrode was fixed at 2.5 mm to ensure a regular arc throughout the test. Arc shielding gas was evaluated with a flow rate of 12 l/min and negative polarity for all experiments. Figure 2 shows the schematic representation of the coating process. Table 1 shows the production condition for NiCrBSi-B_4C coating. The production parameters such as heat input and screening rates were changed to obtain the optimum condition to produce a suitable coating layer that has a sufficient bonding with the substrate. A single TIG arc scanning was performed on each previously placed steel substrate in accordance with the experimental planning shown in Table 1.

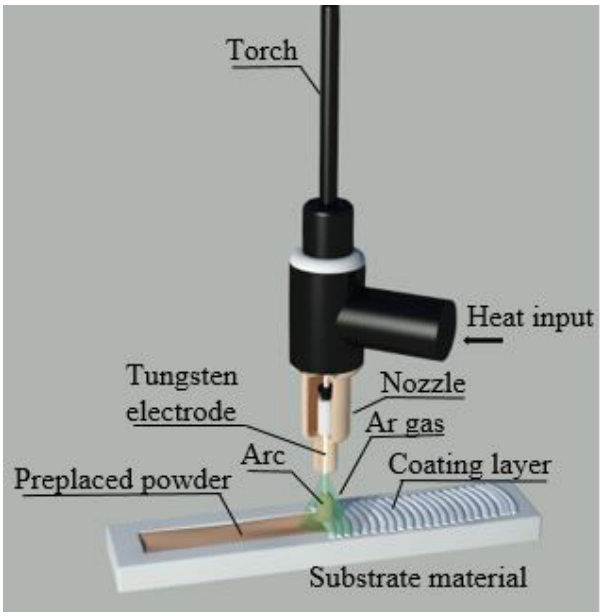

Fig. 2. Schematic diagram of the TIG coating process [14]

In order to analyze the coating morphology, samples were cut in the cross-section direction of the arc scanning. The cross-section of the samples was metallurgically polished with SiC sandpaper with different degrees, followed by diamond paste (average grain size: 1 μm) and polishing felt. These polished samples were etched with 20 ml HCl + 5 gr FeCl3-H2O + 96 ml methanol solution for approximately 3 seconds and the surface morphology was examined. Nikon Eclipse MA200 brand optical microscope was used to examine the distribution of microstructure and hard phases in the structure. In order to analyze the microstructure of the coating, TESCAN MIRA3 XMU and energy dispersive spectrometry (EDS) analyses were performed from the cross section of the coating. Microhardness value of the coating was measured using Future Tech FM-700 microhardness tester under 50 gf load for 10 seconds. The average microhardness values of the coating were recorded by taking the arithmetic mean of 9 measurements taken from random regions from the cross-section of the coating. In order to evaluate the various compounds forming in the coating layer, X-ray diffraction (XRD) technique was used for all coating samples produced in different parameters. XRD was performed with the help of Rigaku RadB-DMax II diffractometer using cobalt target (λ = 1.79026 Å) by considering 20-90° scanning range, 0.02° step size and 10° scanning speed per minute.

3. Results and Discussion

Figure 3 shows macro image and lateral section microstructure of NiCrBSi-B_4C composite coating. As seen in macro-photographs, top surface of the coating was smooth and protruding while its width was 10 mm and the maximum depth was 1.85 mm. The optical microstructure image in Figure 3 shows that the coating layer was made of dense dendrite structures. Dendrites developed perpendicular to the interface region. In addition, the intermetallic white layer between the coating layer and substrate was determined as a line separating the coating from the substrate. It is stated that the intermetallic layer forming after the powders plastered on the substrate and its surface were simultaneously melted and solidified with an external energy affected the metallurgical bonds between the materials [15]. During the crystallization process, dendrite first precipitates from the liquid phase with high cooling rates (high cooling) and finally the eutectic structure forms at the grain boundaries [16]. It was observed that the interface line forming

TABLE 1

Details of the experimental conditions for TIG coating

Electrode: Thorium Tungsten (2.4 mm diameter) Polarization: DCEN Average arc volt/Current : 10-12 V/ 105 A Shielding gas: Argon (12 l/min)				
Experiment No	**Sample label**	**Wt.% B_4C Powder**	**Production speed (mm/s)**	***Heat input (kJ/mm)**
S1	NiCrBSi	—	0.655	0.910
S2	NiCrBSi-wt.% 5 B4C	5	0.776	0.780
S3	NiCrBSi-wt.% 10 B4C	10	0.842	0.718
S4	NiCrBSi-wt.% 15 B4C	15	0.769	0.786

* Heat input Q = η.U.I/s, U: volt, I: current, s: production speed, η: coefficient (η = 0.48 for TIG process)

between the coating layer and the substrate formed in the form of a smooth band. The coating layer was metallurgically well bonded and also had a non-porous structure without any crack.

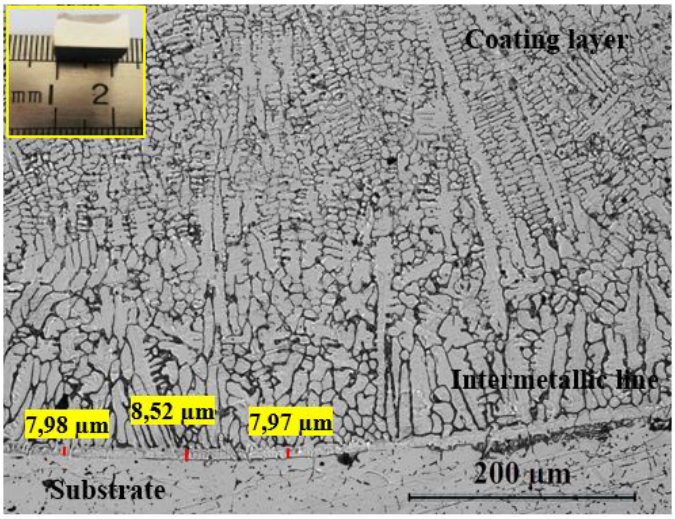

Fig. 3. Macro image and optical microstructure of NiCrBSi coating layer-intermetallic layer-substrate (X500)

X-ray diffraction tests were conducted on the coating layer to investigate the phase structure of NiCrBSi/B_4C MMC coating layers and shown in Figure 4. It was observed that B_4C phase did not exist in XRD patterns. The melt pool decomposed B_4C into B and C elements and allowed new hard phases to form. In addition, along with B_4C, matrix element NiCrBSi and substrate atoms also decompose in the melt pool. These decomposed atoms form new phases with solidification. Cr_7C_3, γ – Ni phases formed at the high peak forming at an angle of 45°. CrB phase was also in the structure at low peaks between the angles of 55-60° degrees. It was determined as a result of XRD analysis that while Cr_7C_3, γ – Ni and CrFeB phases had high peaks, Ni_3B, CrB and Fe_2B phases had low peaks. It was determined that similar results were also obtained in the studies conducted by Meng, Zhou and other researchers [17-20].

Figure 5a-d shows the lateral section optic microstructures of the coating samples produced with different parameters. In the upper region of the coating layers, the dendrites, constituting the microstructure of the coating, solidified in an outward direction [21]. It was observed that NiCrBSi coating layer produced with high production speed was composed of a dendrite dense structure (Fig. 6a). Dendritic structures (white phase) and eutectic structures (black phase) formed in samples produced by adding B_4C (Fig. 6b-d). While dendrites forming in the structure were seen in cellular structure in Figure 6b and c, they formed in columnar and branched form in Figure 6d. Since the temperature gradient (G) is high and the solidification rate (R) is relatively low at the bottom of the molten pool, solidification starts from the substrate surface without nucleation. As the solid/solution interface progresses along the plane, dendritic structures are formed due to the decrease of G/R in the solidification structure [22].

Figure 6a-b and Figure 7a-b show SEM images of NiCrBSi and NiCrBSi-B_4C coatings. Table 2 and Table 3 show EDS results of coatings. It is clear that the NiCrBSi coating layer shown in Figure 6a was composed of dark gray eutectics and light gray dendritic structures. Dendrite structures formed in a cellular structure. Accelerated solidification by rapidly decreasing temperature in the melt pool depending on high feed rate of 122 mm/sec. led the dendrites to solidify without elongating.

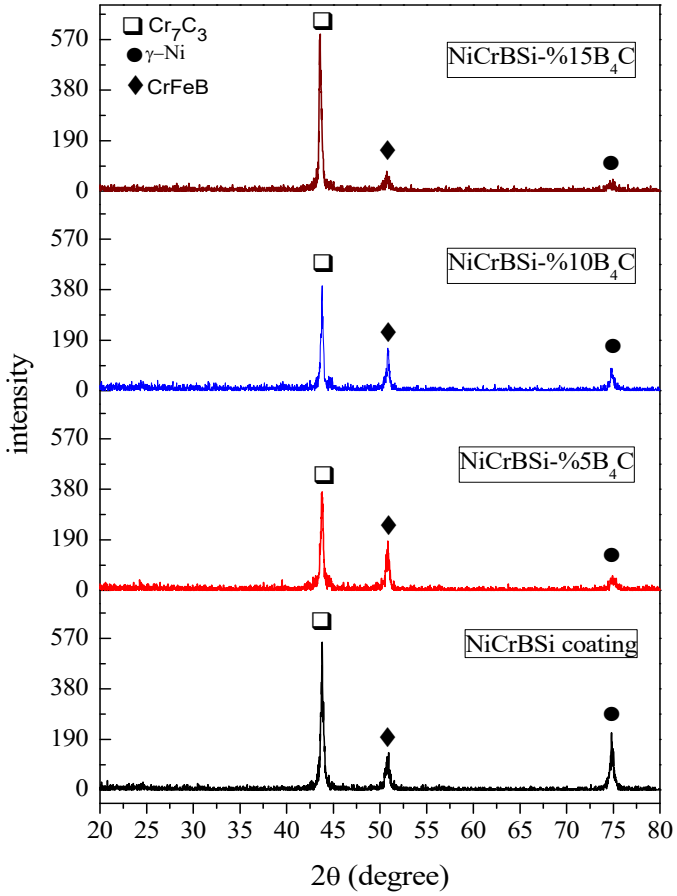

Fig. 4. XRD spectra of NiCrBSi and NiCrBSi/B_4C composite coatings

The coating layer contained Fe, Ni, B, Cr, C and low rates of Si and Mn elements. Cr, Fe and Ni in the melt pool were dissolved together in the melt pool to form more than one liquid. Fe and Cr elements in the dissolved liquid can react with B and form phases such as Fe_2B and CrB [23]. Besides, it is thought that high amount of chromium and boron elements in the dark gray structures in the eutectic regions contribute to the formation of chromium boride phases. The analysis result of the point number 4 taken in the dark gray region in the EDS results of S1 sample given in Table 2 was 15.25 wt.% B, 6.93 wt.% C, 0.75 wt.% Si, 28.95 wt.% Cr, 0.88 wt.% Mn, 37.96 wt.% Fe and 9.28 wt.% Ni, respectively. It was determined in the EDS result of the point number 5 that there were 15.51 wt.% B, 6.37 wt.% C, 0.92 wt.% Si, 22.83 wt.% Cr, 0.97 wt.% Mn, 39.86 wt.% Fe and 13.53 wt.% Ni, respectively. As seen in the EDS results of the dark gray regions representing the eutectic structure, B, C and Cr elements solidified more intensely, especially in the upper and middle parts of the melt pool. It was also determined from

no. 2 and no. 7 EDS analysis results that Fe and Ni were more dense in the dendrite structures in the upper and bottom parts of the coatings (Table 1). In the EDS results taken from the light gray structures representing the dendrite structures of the same sample, the point number 2 was 3.26 wt.% B, 5.84 wt.% C, 1.55 wt.% Si, 11.84 wt.% Cr, 0.76 wt.% Mn, 51.18 wt.% Fe, and 25.58 wt.% Ni, respectively. In the EDS results of the point number 7, 0.38% B, 2.34% C, 0.59% Si, 16.62% Cr, 1.27% Mn, 66.30% Fe and 12.49% Ni elements were determined. While the substrate elements Fe, C and Mn diffused towards the coating layer, it was determined in the EDS results that the coating elements B and Ni successfully diffused toward the coating layer. In the light of these data, it can be asserted that a good metallurgical bond formed between the coating layer and the substrate.

Figure 7b shows SEM images of 5% B_4C reinforced S2 sample. As in the S1 sample, the coating layer was composed of dendritic structure and the eutectic structures between dendrites. It was observed that the solidification of the melt pool was slower since its feed rate (103 mm/sec) was slower than S1 sample and thus the dendrite arms solidified longer. No defects such as pores and cracks were found in the coating layer as in the S1 sample. As seen from the EDS analysis results, B and C elements were denser in the middle and top sections of the coating in the element distribution. Especially in the no. 6 EDS analysis result taken from the point similar to the black particle, B and C exhibited high values by weight. The elements emitted affected the microstructure and properties of the interface due to the concentration gradient of the interface elements during the melting in the coating process made with TIG method [24]. With the change of these values, the alloying elements coming from the substrate and the powder transferred to the surface can form a new composite layered region having different structure and composition [25]. Table 1 shows EDS results of B_4C reinforced S2 coating. In the no 4, 5 and 6 EDS results taken from the eutectic structures, B and C elements were concentrated mostly in the middle and upper part of the coating, as in the S1 sample. It is believed that B_4C decomposed in the melt pool and exhibited solidification while moving towards the top surface of the pool. It was also confirmed in XRD analysis results that elements such as Cr, N and Fe in the structure formed hard carbide and boride phases with solidification (Fig. 4). It was determined from the microhardness measurement results that these hard boride and carbide phases increased the hardness

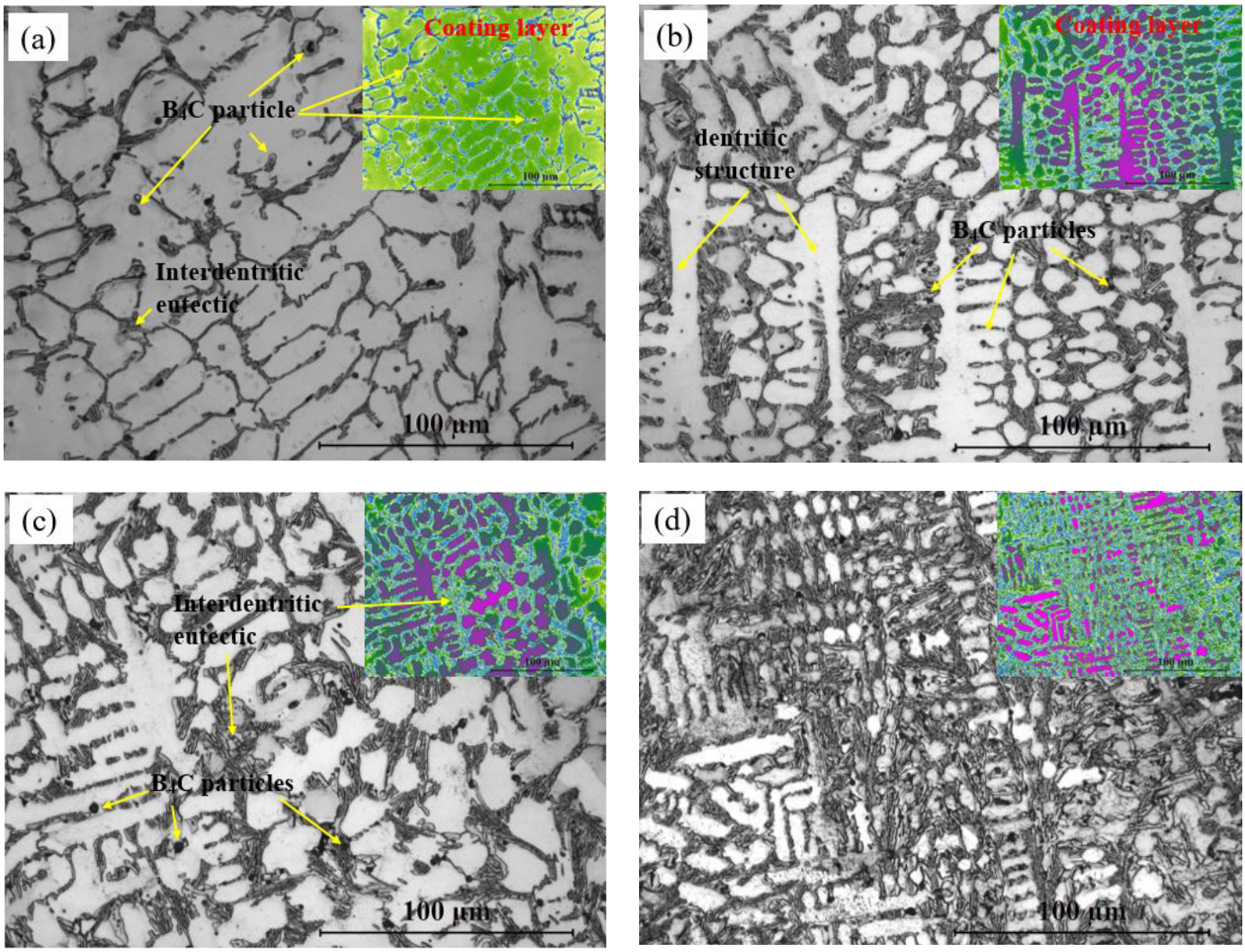

Fig. 5. Lateral section optical microscope image of S1 (a), S2 (b), S3 (c) and S4 (d) coatings

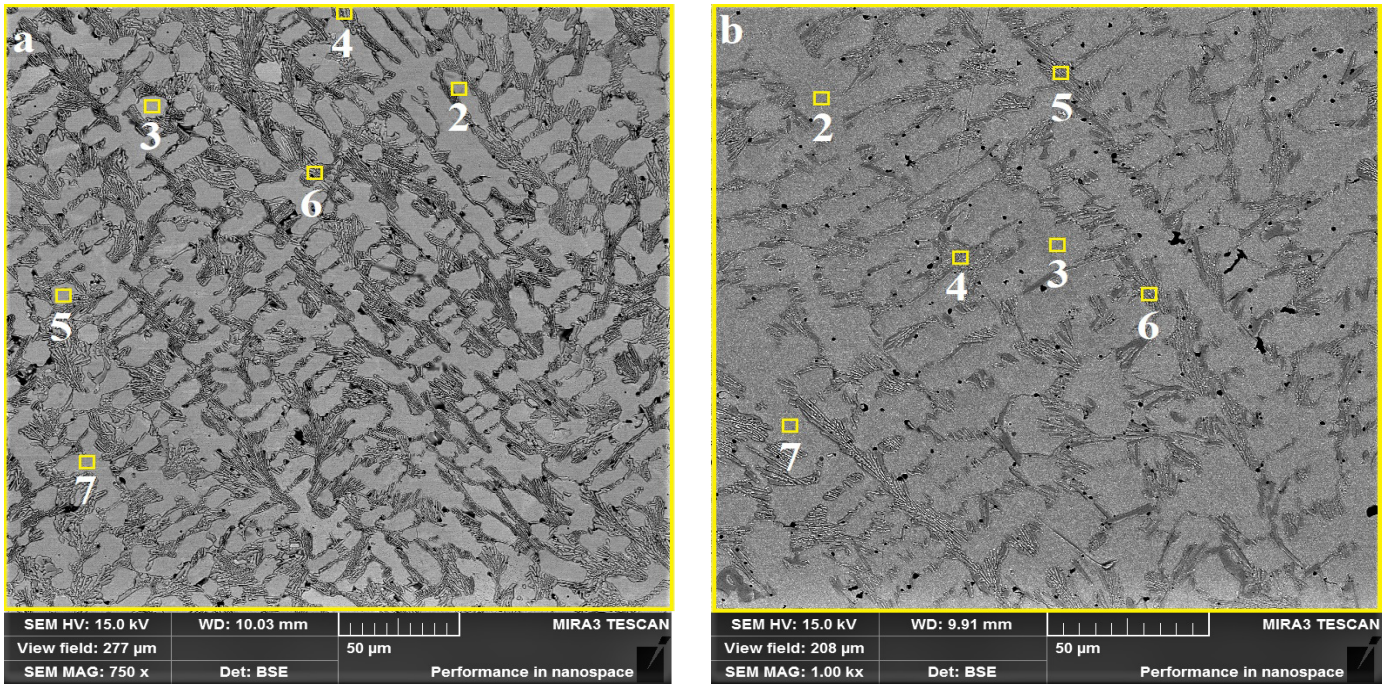

Fig. 6. Lateral section SEM images of S1 and S2 coating samples

of the coating layer (Fig. 8). In the EDS analysis results of the point number 7 representing the region of coating layer close to the interface, there were 1 wt.% B, 2.48 wt.% C, 1.36 wt.% Si, 13.28 wt.% Cr, 0.90 wt.% Mn, 53.17 wt.% Fe and 27.80 wt.% Ni elements, respectively. It can be asserted as a result of EDS analysis, Ni precipitated toward the substrate and contributed to the formation of Fe and γ – FeNi phases. EDS data taken from the point number 6 representing the eutectic region were 53.43 wt.% B, 17.98 wt.% C, 0.25 wt.% Si, 7.43 wt.% Cr, 0.63 wt.% Mn, 14.22 wt.% Fe and 6.06 wt.% Ni, respectively. It was determined from the EDS analysis results that eutectic regions exhibited structures rich in terms of B and C.

TABLE 2

EDS analysis results for S1 and S2 coating samples

Samples	Spectrum	Chemical composition (wt.%)						
		B	C	Si	Cr	Mn	Fe	Ni
S1 (a)	1	12.23	9.97	1.17	17.34	0.90	41.42	16.97
	2	3.26	5.84	1.55	11.84	0.76	51.18	25.58
	3	6.24	8.71	1.56	11.28	0.79	47.32	24.10
	4	15.25	6.93	0.75	28.95	0.88	37.96	9.28
	5	15.51	6.37	0.92	22.83	0.97	39.86	13.53
	6	9.35	2.95	1.09	23.37	1.02	44.36	17.87
	7	0.38	2.34	0.59	16.62	1.27	66.30	12.49
S2 (b)	1	7.44	4.03	1.30	15.51	0.83	45.47	25.43
	2	3.37	2.43	1.44	12.76	1.05	49.96	28.98
	3	2.57	3.13	1.26	12.88	0.79	50.24	29.14
	4	21.70	7.53	0.60	21.13	0.67	33.90	14.47
	5	14.35	6.61	0.87	20.20	0.91	38.81	18.26
	6	53.43	17.98	0.25	7.43	0.63	14.22	6.06
	7	1.00	2.48	1.36	13.28	0.90	53.17	27.80

Figure 7a-b shows SEM images of the NiCrBSi coating sample reinforced with 10% B_4C (S3) and 15% B_4C (S4). Dendritic structures forming the coating layers exhibited a different structure compared to the samples S1 and S2. The dendritic structures in S3 and S4 samples had a more columnar and ring shape structure. The reason for the formation of different structures is believed to be the different feed rate and energy inputs. Table 3 shows EDS analysis results of S3 and S4 coating regions. Along with the solidification of the liquid bath, the diffusion in the solid material changed the distribution of the dissolved elements of the substrate and the coating layer [26]. B_4C ceramic particles in the structure were decomposed into B and C atoms. Since the concentration gradient of B and C atoms with small atomic radii is high at the interface, they can propagate toward the substrate over a long distance. With decomposition, element B can react with the element Fe dissolved from the substrate toward the coating layer and form Fe_2B phase [21,27]. Chromium boride phases can form in situ as a result of the reaction between the elements contained in the matrix element NiCrBSi alloy and the self-flowing matrix element B and Cr atoms [28]. In addition, due to the cavity concentration of metals at high temperature, metal atoms can move easily in cavities and result in the formation of Fe-Ni-Cr solid solution. In this way, dense and completely solid solution allows γ – (Fe, Ni) phase to form at the interface [24]. As seen in the EDS analysis result at the point number 7 taken toward the coating substrate close to the S3 and S4 interface, Fe and Ni concentration was high especially near the interface. It is also supported by the literature that Fe and Ni solid solution in the interface having high concentration formed γ – (Fe, Ni) phase in this zone. Besides, Fe and Ni along with Cr and a small amounts of B, C, Si and Mn were dissolved in EDS results in the same regions. In the EDS analysis data taken in the

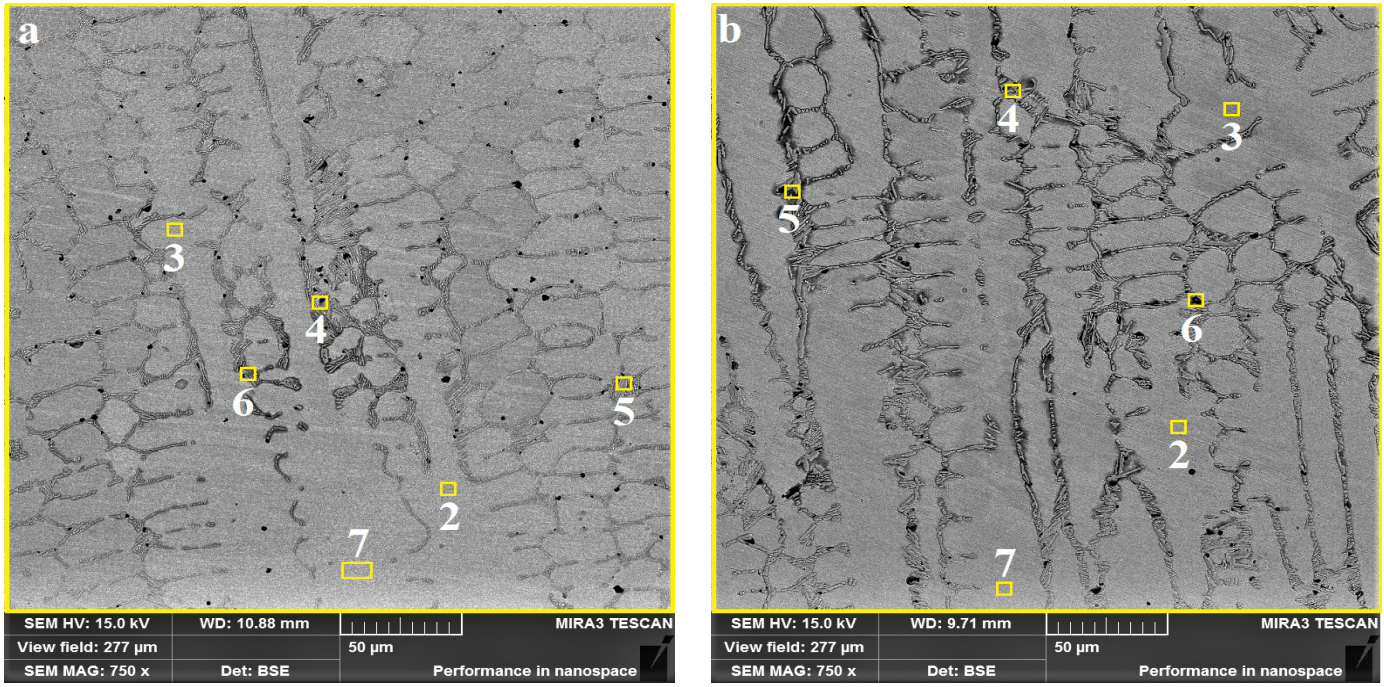

Fig. 7. Lateral section SEM images of S3 and S4 coating samples

eutectic regions especially in the middle and upper parts of the coating in this dissolution area in the melt pool contributed to the precipitation of hard carbide and boride phases such as CrB and Cr_7C_3 depending on the increasing concentration of C and B elements [28]. In fact, as seen in XRD analysis results given in Figure 4, the formation of CrB and Cr_7C_3 phases confirms this result.

TABLE 3

EDS analysis results for S3 and S4 coating samples

Samples	Spectrum	Chemical composition (wt.%)						
		B	C	Si	Cr	Mn	Fe	Ni
S3 (a)	1	7.52	4.88	1.28	14.73	1.04	46.44	24.11
	2	1.16	2.32	1.29	14.57	0.84	52.14	27.68
	3	3.88	3.03	1.18	14.53	0.91	49.84	26.64
	4	16.42	4.97	0.77	26.04	1.12	35.45	15.24
	5	15.18	5.01	0.89	23.28	0.95	37.48	17.21
	6	32.13	6.31	0.74	12.83	1.19	29.96	16.83
	7	2.75	2.47	0.70	16.26	1.01	61.54	15.28
S4 (b)	1	6.54	7.50	1.08	14.87	0.93	46.18	22.90
	2	1.26	2.32	1.17	14.55	0.91	53.90	25.89
	3	2.86	2.57	1.07	14.46	1.02	53.29	24.74
	4	14.41	14.23	0.83	18.00	0.84	35.58	16.12
	5	16.75	21.39	0.62	18.98	0.92	28.74	12.59
	6	28.44	22.99	0.20	21.12	0.63	21.41	5.19
	7	3.99	2.89	0.75	15.72	0.85	58.88	16.91

Figure 8 shows measurement results of microhardness values of NiCrBSi and NiCrBSi-B_4C coatings. Hardness measurements were measured from 9 random points in total from the substrate towards the center of the coating and their arithmetic

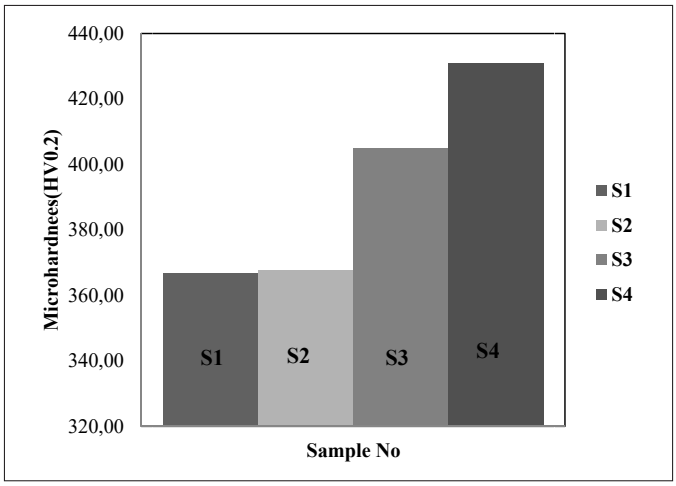

Fig. 8. Microhardness graph of NiCrBSi-B4C composite coatings

means were taken. While the hardness value of the S1 sample coated with NiCrBSi was 366.9 $HV_{0.2}$, quite high values were recorded in hardness with B_4C additions. The hardness measurement values obtained from the coating layer of the B_4C reinforced samples S2, S3 and S4 were resulted as 367.8 $HV_{0.2}$, 405 $HV_{0.2}$ and 430.8 $HV_{0.2}$. Depending on the results, it was also determined from the measurement results that the hardness of the coating layer increased by 2-2.5 times compared to the hardness of the substrate with increasing rate of B_4C reinforcement. Another reason for this increase can be associated with the increase in the coating hardness of hard phases such as Cr_7C_3, Ni_3B, and CrB forming in the structure as a result of the distribution of Ni and Cr into the substrate during melting process [27]. In addition, as another reason for this hardness increase, dense dendrite and/or fine-particle size structures forming in the structure with the

rapid solidification in the melt pool play an important role in the increase of the hardness of the coating material depending on the production speed [29].

4. General conclusions

With TIG method, NiCrBSi and NiCrBSi-B_4C composite coating layers were produced on the surface of AISI 304 stainless steel surface. The following results were obtained;

1. NiCrBSi matrix and reinforcement B_4C elements were dissolved with high-energy input and CrFeB, Ni_3B, CrB, Fe_2B and Cr_7C_3 carbide and phases formed respectively by diffusion of elements during solidification.
2. An intermetallic layer formed between the coating layer and the substrate.
3. Hardness measurements increased depending on the increase in the ratios of B_4C alloy. According to this, while the highest hardness value was obtained in the coating layer of S4 sample (430.8 $HV_{0.2}$), the lowest hardness value was recorded from the sample S1 (366.9 $HV_{0.2}$) The microhardness value of the coating layer was 2-2.5 times greater compared to the microhardness value of the substrate.

REFERENCES

[1] R. Rachidi, B. El Kihel, F. Delaunois, Mater. Sci. Eng. B-Adv. **241**, 13-21 (2019).

[2] H. Zhao, J. Li, Z. Zheng, A. Wang, D. Zeng, Y. Miao, Surf. Coat. Tech. **286**, 303-312 (2016).

[3] C.K. Sahoo, M. Masanta, J. Mater Process Tech. **240**, 126-137 (2017).

[4] Q. An, L. Huang, S. Jiang, X. Li, Y. Gao, Y. Liu, L. Geng, Vacuum. **145**, 312-319 (2017).

[5] J.-S. Meng, G. Jin, X.-P. Shi, Appl. Surf. Sci. **431**, 135-142 (2018).

[6] S. Buytoz, M. Ulutan, M.M. Yildirim, Appl. Surf. Sci. **252**, 1313-1323 (2005).

[7] J. Yin, D. Wang, L. Meng, L. Ke, Q. Hu, X. Zeng, Surf. Coat. Tech. **325**, 120-126 (2017).

[8] J. Rodriguez, A. Martín, R. Fernández, J.E. Fernández, Wear. **255**, 950-955 (2003).

[9] N.L. Parthasarathi, M. Duraiselvam, J. Alloy Compd. **505**, 824-831 (2010).

[10] S. Abdi, S. Lebaili, Phys. Procedia. **2**, 1005-1014 (2009).

[11] M.J. Tobar, C. Álvarez, J.M. Amado, G. Rodríguez, A. Yáñez, Surf. Coat. Tech. **200**, 6313-6317 (2006).

[12] N.Y. Sari, M. Yilmaz, Surf. Coat. Tech. **202**, 3136-3141 (2008).

[13] E. Fernández, M. Cadenas, R. González, C. Navas, R. Fernández, J. de Damborenea, Wear **259**, 870-875 (2005).

[14] S. Buytoz, GU J. Sci., Part C. **8**, 51-63 (2020).

[15] X.-N. Wang, X.-M. Chen, Q. Sun, H.-S. Di, Mater. Lett. **206**, 143-145 (2017).

[16] K.A. Habib, D.L. Cano, José Antonio Heredia, J.S. Mira, Surf. Coat. Tech. **358**, 824-832 (2019).

[17] L.-Y. Chen, T. Xu, H. Wang, P. Sang, L.-C. Zhang, Surf Coat Tech. 358, 467-480(2019).

[18] Q.W. Meng, T.L. Geng, B.Y. Zhang, Surf. Coat. Tech. **200**, 4923-4928 (2006).

[19] Y.-X. Zhou, J. Zhang, Z.-G. Xing, H.-D.Wang, Z.-L. Lv, Surf. Coat. Tech. **361**, 270-279 (2019).

[20] M. Kilic, A. Imak, I Kirik, JMEPEG. **30**, 1411-1419 (2021).

[21] K. Kılıçay, S. Buytoz, M. Ulutan, Surf. Coat. Tech. **397**, 125974 (2020).

[22] M.-J.Chao, X. Niu, B. Yuan, E.-J. Liang, D.-S. Wang, Surf. Coat. Tech. **201**, 1102-1108 (2006).

[23] Y. Z., T. Yu, L. Chen, Y. Chen, C. Guan, J. Sun, Ceram. Int. **46**, 25136-25148 (2020).

[24] L. Guo-lu, L. Ya-long, D. Tian-shun, F. Bin-Guo, Wang Hai-dou, Zheng Xiao-dong, Zhou Xiu-kai, Vacuum. **156**, 440-448 (2018).

[25] S. Buytoz, M. Ulutan, M.M. Yıldırım, Eng. & Arch. Fac .Osmangazi University **XVIII**, 93-107 (2005).

[26] M. Kilic, European Journal of Technique (EJT) **10**, 106-118 (2020).

[27] Guo-lu Li, Ya-long Li, Tian-shun Dong, Hai-dou Wang, Xiao-dong Zheng, Xiu-kai Zhou, Hindawi Advances in Materials Science and Engineering 2018, Article ID 8979678, 1-10 (2018).

[28] M. Storozhenko, O. Umanskyi, V. Krasovskyy, M. Antonov, O. Terentjev, J. Alloy Compd. **778**, 15-22 (2019).

[29] A. Zabihi, R. Soltani, Surf. Coat. Tech. **349**, 707-718 (2018).